Short Circuit Fault Modeling of Squirrel Cage Induction Generator - ECE 711 Project

Gokhan Cakal, David Skrovanek

I. Abstract

A line-fed squirrel cage induction wind turbine generator was modelled and simulated in MATLAB Simulink. The short circuit behavior of the machine was studied by conducting two short circuit test scenarios during rated operation. Results indicate that the rotor speed will increase due to the imbalance between applied turbine torque and the machine's electromagnetic torque. In addition, the phase currents of the machine increased by as much as 7 pu, highlighting just one of the non-idealities in real-life generator operation. The phase currents for the three-phase short circuit were also derived analytically and it was found that the peak phase current matched within 5% of the simulation results. This work provided the authors with good experience in studying wind turbine generators.

II. Introduction

While squirrel cage induction generators (SCIG) are slowly being replaced by permanent magnet synchronous machines for wind energy applications, they still represent a sizable portion of today's installed wind capacity and continue to be researched for future wind turbine technology. As such, this paper investigates the transient behavior of SCIG wind turbines during various short circuit conditions. These short circuit faults typically arise due to moisture, mechanical stress, deterioration of turn-to-turn windings, and can damage system components [1]. Specifically, two short circuit case scenarios are developed in this paper via simulation; the first being a three-phase short of the machine stator windings to ground and the second being a two-phase short between two of the stator's phases. In each scenario, the maximum torque and maximum phase currents are calculated and analyzed. Additionally, the effect of the complex voltage vector position on fault characteristics is investigated. For the three-phase short circuit, the peak amplitude, frequency, and decay of the phase current are also determined analytically, using the trapped flux approximation.

III. System Description

A. Induction machine model

The parameters for the SCIG can be found in Table I. In the simulation, all parameters were per-unitized and all calculations were performed as such. Higher-order effects such as saturation, skin-effect dependencies, and thermal dependencies were ignored for simplicity's sake. It is also assumed that the SCIG is excited by the grid (i.e. line-fed), so an inverter model was not needed. A simple mechanical model was used that neglects the aerodynamics and mechanics of the wind turbine and just assumes that drag, friction, and other effects are already included in the load torque applied to the generator.

The qd stator and rotor voltage equations in an arbitrary reference are expressed below

$$v_{qds} = r_s \underline{i}_{qds} + L_s \left(p + j\omega\right) \underline{i}_{qds} + L_m \left(p + j\omega\right) \underline{i}_{qdr} \quad (1)$$

$$v_{qdr} = r_r \underline{i}_{qdr} + L_r \left(p + j\left(\omega - \omega_r\right)\right) \underline{i}_{qdr} + L_m \left(p + j\left(\omega - \omega_r\right)\right) \underline{i}_{qds} \quad (2)$$

where v_{qds} is the qd stator voltage; v_{qdr} the qd rotor voltage; i_{qds} the qd stator current; i_{qdr} the qd rotor current; L_s, L_r, and L_m the stator, rotor, and mutual inductances, respectively; ω the frequency of the arbitrary reference frame; ω_r the electrical rotor speed; and p the derivative operator.

The mechanical equation is given as

$$J\frac{d\omega_{rm}}{dt} + T_l = T_e = \frac{3P}{4}\Im\left[\underline{i}_{qds}\underline{i}^*_{qdr}\right] \quad (3)$$

where J is the inertia of the shaft; T_l and T_e the electrical and load torque, respectively; and P the pole count.

B. Simulink Implementation

For the fault analysis, the squirrel-cage induction generator is modeled in MATLAB Simulink, shown in Fig. 1. The short circuit fault is takes place within the green block of the figure. It executes the fault when the trigger signal is applied.

The inside of the main machine block is shown in Fig. 2. The SCIG is modeled using flux-voltage equations. The equations are solved in the synchronous frame. As such, the ABC/DQ and DQ/ABC conversion blocks can be found in

Table I
Squirrel-cage induction generator parameters

Symbol	Description
Parameter	*Value*
Rated output power	1.45 MW
Rated phase voltage	331.98 V (rms)
Rated current	1723 A (rms)
Rated frequency	50 Hz
Rated rotor speed	1007.2 rpm
Rated slip	-0.0072
Number of pole pairs	3
Rated torque	13.944 kNm
Stator winding resistance	1.354 mΩ
Rotor winding resistance	1.39 mΩ
Stator leakage inductance	0.1044 mH
Rotor leakage inductance	0.0498 mH
Magnetizing inductance	1.77016 mH

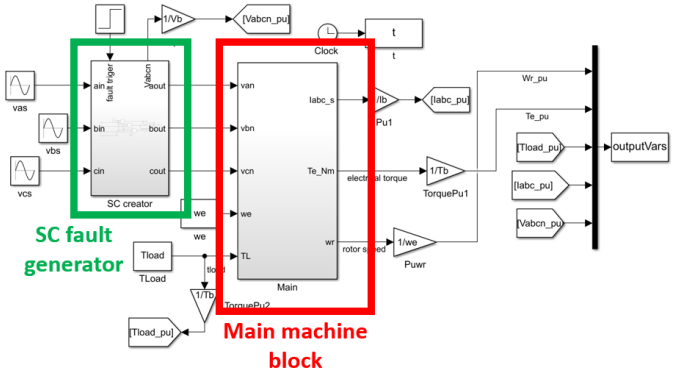

Figure 1. SCIG short circuit fault model on Simulink

the model. The rotor speed is calculated by Eqn. (3) inside the blue block in the figure. The flux-voltages, D-axis stator current, Q-axis stator current, and torque are calculated using the machine equations within the other blocks.

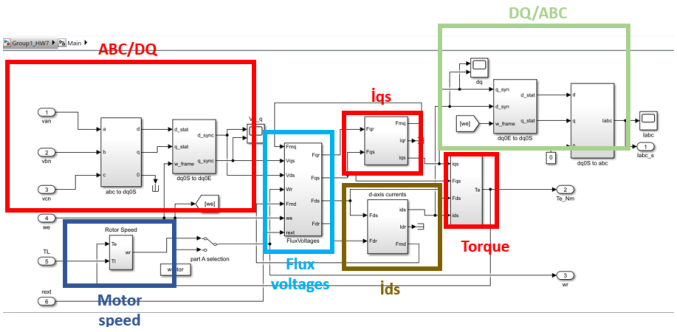

Figure 2. Main components of the SCIG machine block in Simulink

Using the introduced Simulink model of the SCIG, the linear torque-speed region of the SCIG is obtained as shown in Fig. 3. To achieve torque speed characteristics of the SCIG, the load torque is varied between -2 pu and 2 pu, and steady state speed of the machine is recorded. All simulations took place within the linear region, as torques exceeding the linear range (roughly [-2,2] pu) would lead to instability. The rated operating point of the generator is shown with a star on the torque-speed characteristics.

IV. Short Circuit Analysis

Two short circuit scenarios were evaluated in this project. In the first case, all three phases were short circuited at the stator terminals of the SCIG. In the second case, only two phases were short circuited at the stator terminals. Under both fault conditions, the machine was assumed to be operating under constant rated load torque. The generator was driven by the turbine and the operating torque was set to -1 pu. The speed of the generator was determined by the difference between the turbine torque and generator torque as well as the inertia of the overall system as dictated by Eqn. (3).

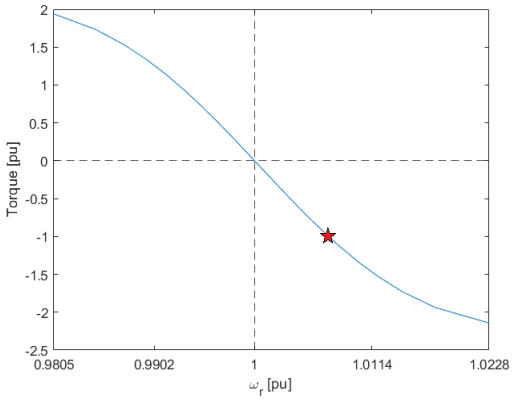

Figure 3. Linear region of the torque-speed curve for the SCIG

A. Three Phase Short Circuit - Simulation

For the three phase short circuit study, all stator phase terminals of the machine were short circuited at $t = 2.5s$. This time was selected such that the machine would be operating at steady state conditions before the fault. Initially, the fault was applied when V_a is maximum. In other words, it is assumed that the complex voltage vector is aligned with V_a when the fault was applied. The short circuit characteristics are shown in Fig. 4.

The short circuit scenario can be seen from the phase voltages plot in Fig. 4. After the fault, all of the phase voltages became zero, representing the three phase short circuit. From the torque plot in the same figure, it can be seen that the steady state torque of the generator after the fault was zero. This can be explained by the nature of the SCIG topology. Since the rotor is composed of short-circuited bars, there is no source of excitation at the rotor. The machine excitation is achieved by the stator excitation. Since there was a three phase short circuit, there is no remaining source of flux in the machine after the fault at steady state. Therefore, zero torque was observed for the machine following the fault (except during the transient).

After the fault, the load torque from the turbine did not change; however, the generator torque converged to zero. This caused the rotor speed to increase, as seen in the speed plot in Fig. 4. In the plot, the mechanical speed increases up to 1.06 pu; however, it will keep increasing towards infinity until some mechanical fault occurs or mechanical break is applied by the system. Usually for wind turbine systems, the generator and turbine should be mechanically decoupled for this kind of fault to prevent speed runaway.

For the fault phase currents, the peak current was about six times greater than the rated current. The fault currents converged to zero after transient oscillations due to the same reason that there is no source of excitation after three phase short circuit fault.

The next part of this work investigated the effect of the fault timing on fault characteristics, where fault timing refers to the position of the voltage vector at the instant of the fault.

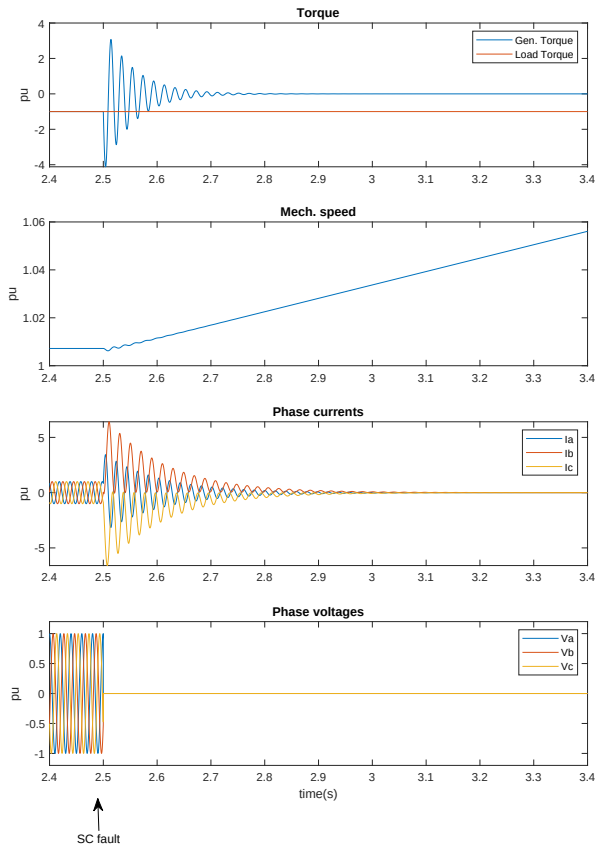

Figure 4. Three phase short circuit fault characteristics when Va is maximum

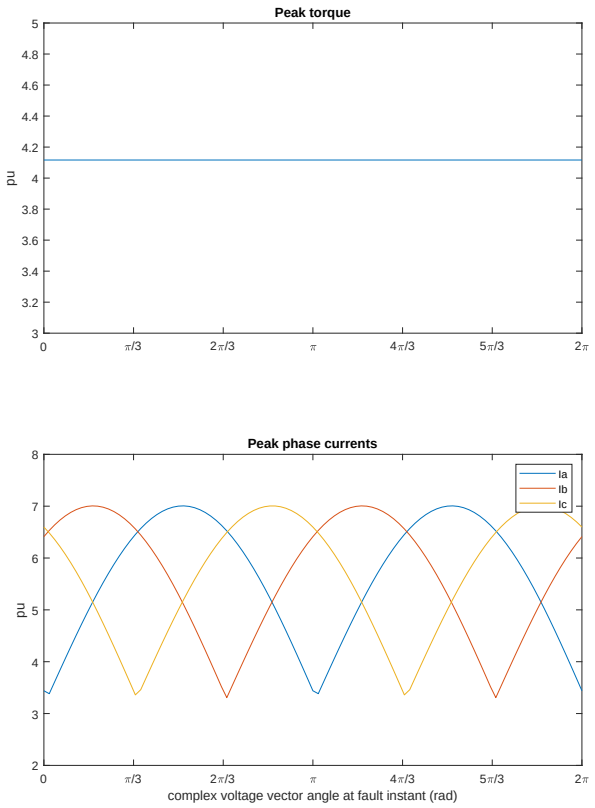

Figure 5. The effect of complex voltage vector angle on three phase fault characteristics

The fault characteristics shown in Fig. 4 are obtained when V_a is maximum, i.e. the complex stator voltage vector, $\underline{V}^s_{qds}$, is aligned with V_a. However, this may not be the case always for a short circuit fault. It would seem reasonable to assume that the angle of the complex stator voltage vector would effect the short circuit characteristics. In order to investigate this, the fault time was applied at 100 different equally-spaced instants within a single electrical period. This corresponds to 100 equally-spaced angles for the complex stator voltage vector in the range of 0 to 2π. In these simulations, the peak transient torque and peak transient phase currents were obtained and plotted in Fig. 5 as a function of complex stator voltage angle.

The results show that the peak transient torque is independent of the complex stator voltage angle. This can be explained by the torque equation in Eqn. (4).

$$T_e = \frac{3P}{4} \Im \left[\underline{i}^e_{qds} \underline{i}^{e*}_{qdr} \right] \tag{4}$$

Since the complex stator and rotor currents, $\underline{i}^e_{qds}$ and $\underline{i}^{e*}_{qdr}$ are independent of the complex stator vector angle, it can be predicted that the short circuit torque characteristics will also be independent of the complex stator vector angle.

Contrary to torque, it can be seen that the phase peak currents at the three phase fault depends on the complex stator vector angle. Depending on the three phase fault instant, the peak phase current may change between 3 pu and 7 pu. In the literature, a typical peak short circuit current for a SCIG is reported as 5-6 pu depending of the size of the generator [2], which is consistent with the results of this study.

For the angle span of 0 to 2π, there are two peaks for each phase. For example, for phase A, the peak transient current is observed when the complex voltage vector is at roughly $\pi/2$ and $3\pi/2$. This corresponds to $\pi/2$ ahead and behind of V_a, respectively. Thus, it can be concluded that the peak fault current at any given phase is not observed when the complex voltage vector is aligned with that phase at the fault instant. It is instead observed when the complex voltage vector is $\pi/2$ ahead and behind of the phase.

B. Three Phase Short Circuit - Analytical Calculations

For very short intervals following a disturbance, the damping of transient solutions can be ignored and a simpler analysis under the assumption of constant rotor flux linkage (i.e. constant "trapped flux") can be employed to determine short circuit current behavior. This technique also hinges upon the assumption that the rotor speed is constant, which is a reasonable approximation for this machine, given its large moment of inertia.

By declaring

$$\lambda_{qdr} = \lambda_{qdr0} e^{-j(\omega-\omega_r)t} \tag{5}$$

in the arbitrary reference frame, the equivalent circuit in Fig. 6 can be derived. This circuit introduces $L_s^{'}$ which is the stator transient inductance and is given by the product of the stator inductance L_s and leakage factor σ. $E_{qd}^{'}$ represents the voltage behind transient reactance and can also be thought of as the trapped flux voltage. Its steady-state value prior to the disturbance is given by

$$\underline{E}_{qd}^{'} = (1-s)\frac{L_m}{L_r}\underline{E}_{rp} \tag{6}$$

where E_{rp} is the flux voltage across the rotor resistor and can be derived from voltage division on the steady-state model of the induction machine. Because the rotor-side dynamics are ignored, the solution to the differential equation describing the short circuit current will contain only one eigenvalue and will take the form

$$\underline{i}_{qds}^{s} = \underline{C}e^{\lambda t} + \underline{I}_{sc}e^{j\omega_r t}. \tag{7}$$

Because the trapped flux model simplifies the machine into a simple RL circuit, the eigenvalue can be immediately found at $\lambda = \frac{-r_s}{L_s^{'}}$. In the forced solution, $\underline{I}_{sc}$ is simply the short circuit current flowing in the circuit, and can be derived from Ohm's Law as

$$\underline{I}_{sc} = -\frac{\underline{E}_{qd}^{'}}{r_s + j\omega_r L_s^{'}}. \tag{8}$$

To obtain the constant $\underline{C}$ in the natural response, the initial $\underline{i}_{qds}^{s}$ at $t = 0^-$ and $t = 0^+$ must be used in conjunction with the natural response evaluated at those times. At $t = 0^-$, the forced solution is zero and $\underline{i}_{qds}^{s}$ is just the result of Ohm's Law in the trapped flux circuit. At $t = 0^+$, the forced solution is nonzero and is equal to $\underline{I}_{sc}$ and the natural response is just $\underline{C}$. Without ignoring stator resistance and taking into account that $\omega_e \neq \omega_r$,

$$\underline{C} = \frac{\underline{v}_{qds}}{j\omega_e L_s + r_s} + \frac{\underline{E}_{qd}^{'}}{j\omega_r L_s^{'} + r_s}. \tag{9}$$

The analytically determined short circuit current for phase A is plotted in Fig. 7 against the same phase A current from the simulation. It can be seen that the trapped flux model approximates the actual behavior of the transient quite well for the first few cycles, as the peak value of the analytical result differs only by ca. 0.16 pu, or 4.8%. In addition, the frequency of both curves are equal at 50 Hertz with a slight phase shift. Beyond a few cycles though, the trapped flux model can no longer accurately predict the actual phase currents because it assumes the rotor flux to never decay, whereas in reality, the source of the rotor flux disappears following a short circuit as in Fig. 4.

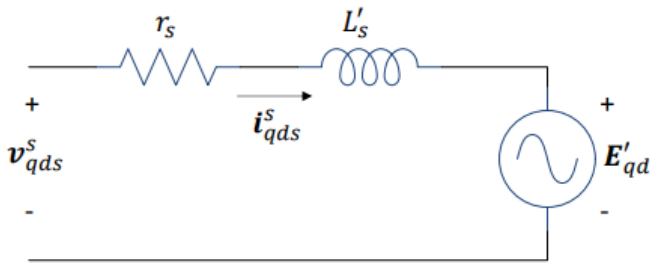

Figure 6. Equivalent circuit under the assumption of constant rotor flux linkage [3]

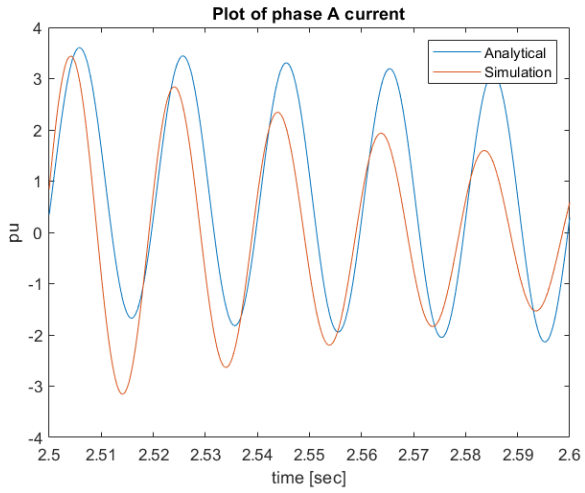

Figure 7. Comparison between phase A short circuit current from analytical and simulation results

C. Two Phase Short Circuit

As a another short circuit fault case study, two phase short circuit characteristics were obtained for the SCIG. As in the case of the three phase fault, the generator is operated at rated torque and steady state before the fault. For this study, phase A and phase B were short circuited to each other at the stator terminals. Similar fault characteristics were expected for the other two phase short circuit situations.

In Fig. 8, the two phase short circuit characteristics were obtained in per unit values. These results are obtained when V_a is maximum. In other words, the complex voltage vector is aligned with phase A when the fault is applied. In the voltage plot in the figure, it is seen that phase A and phase B voltages are set to zero, and phase C is still connected to the generator. Unlike the three phase short circuit case, there is a source of excitation at the machine after the fault by phase C.

The torque plot in Fig. 8 shows that there are steady state oscillations in the torque, and the average torque is close to zero and less than the turbine torque. This difference causes an increase in the speed towards infinity until a mechanical break or fault is observed.

Unlike three phase short circuit fault, the phase currents do not converge to zero for two phase short circuit case, even for

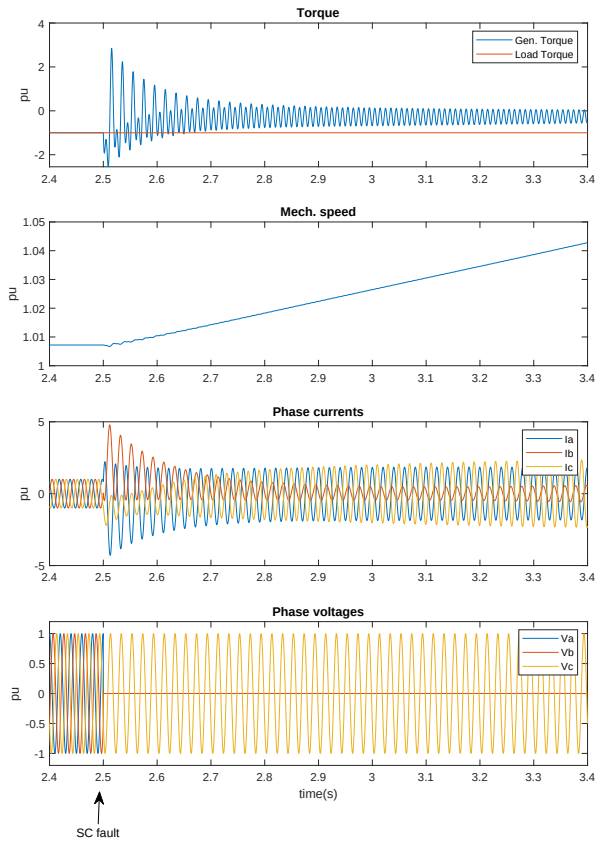

Figure 8. Two phase short circuit fault (AB short circuit) characteristics applied when V_a is maximum

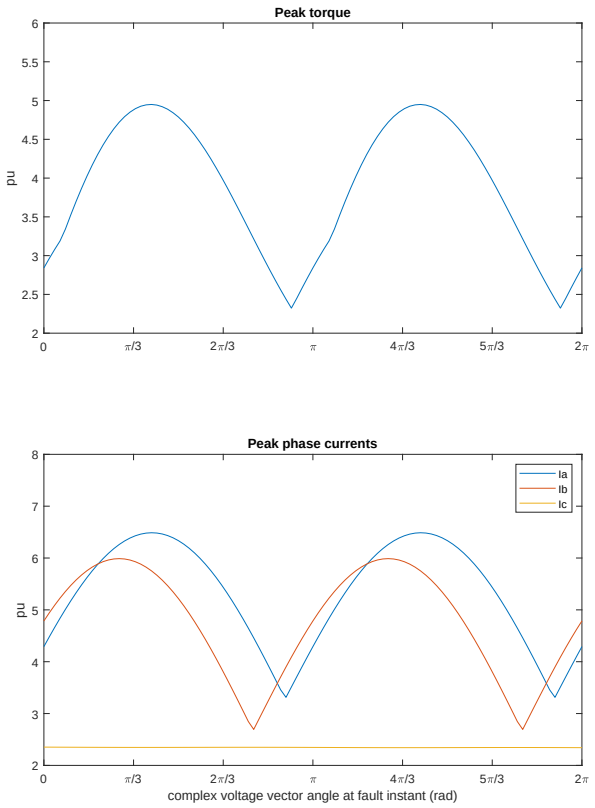

Figure 9. The effect of complex voltage vector angle on two phase (AB) fault characteristics

phase A and phase B which are short circuited. This can be explained by the electromagnetic coupling between the phases.

For this two phase AB short circuit fault, the fault is applied when V_a is maximum. In order to investigate the effect of the complex voltage vector angle on the fault characteristics, the same fault is applied at different instants, and peak torque and peak currents are recorded. The results are plotted in Fig. 9 as a function of the complex voltage vector angle.

The analysis results shows that peak torque varies as a function of complex voltage vector angle, unlike three phase short circuit fault. This can be explained by the unbalanced nature of the two phase short circuit fault. Since there is an unbalanced voltage excitation after the fault, the $\underline{i}^{e}_{qds}$ and $\underline{i}^{e*}_{qdr}$ currents become a function of the complex stator voltage angle. This dependency results in variable peak torque values for different complex stator voltage angles as shown in Fig. 9.

For the peak phase current characteristics in Fig. 9, it is seen that the phase C peak current is independent of the complex voltage vector angle because the short circuit fault happened at the other two phases. Similar to the three phase short circuit fault, two peaks are observed for the phase A and phase B peak fault currents vs. the complex voltage vector angle at the fault instant.

V. Conclusion

Analysis was conducted on a squirrel-cage induction generator operating as a wind turbine in which the transient behavior of the machine was simulated for two different short circuit cases. More specifically, a three phase and a two phase short circuit were applied and the machine's speed, torque, and current response were determined. In both cases, the generator could not produce any average torque following the faults to match the turbine torque from the wind, causing the rotor speed to monotonically increase. Furthermore, this study revealed the dependency of the voltage vector position on the peak torque and peak phase currents. In the case of a three phase short circuit, the peak torque had no dependency but the phase currents are maximized when the voltage vector angle is displaced by $\frac{\pi}{2}$ relative to the phase at the instant of the fault. Peak phase currents reaching as much as 7 times their rated value were observed during the fault. For the two phase short circuit, both the peak torque and phase currents depended on the voltage vector angle.

References

[1] S. et al., "Impact of inter-turn short-circuit fault on wind turbine driven squrrel-cage induction generator systems," 2014.

[2] J. W. Group, "Fault current contributions from wind plants," in *2015 68th Annual Conference for Protective Relay Engineers*, pp. 137–227, 2015.

[3] S. Fredette, “ECE 711 class notes,” 2022.